


Statistical singularity energy in ferroelectric phase transitions

Huijiadai Luo^{1,*}, Lu Cao^{1,*}, Hua Ke^{1,†}, Guangtong Liu², and Yu Zhou^{1,‡}

¹*School of Materials Science and Engineering, Harbin Institute of Technology, Harbin 150001, China*

²*Beijing National Laboratory for Condensed Matter Physics, Institute of Physics, Chinese Academy of Sciences, Beijing 100190, China*

 (Received 21 December 2022; revised 12 May 2023; accepted 18 July 2023; published 4 August 2023)

The ferroelectric phase transitions described by Landau-Devonshire's phenomenological theory can be statistically simulated using the effective Hamiltonian (H_{eff}) based on first-principles calculations. In a Monte Carlo (MC) simulation, we observe a statistical singularity energy caused by a subtle difference between the macroscopic phenomenological model and the microscopic statistical model in the mathematical space of the phase transition point. This statistical singularity energy is measured according to the parameters of the H_{eff} model and introduced by the transition probability of the MC algorithm, which greatly improves the accuracy of the prediction of the phase transition temperatures and restores the true fluctuations near the phase transition point. For the cubic-tetragonal phase transition for BaTiO₃ and PbTiO₃, we obtain a good estimation of the thermal hysteresis corresponding to the experiments. We further reproduce the difference of the phase transitions between heating and cooling sequences, which is verified by the experimental observations.

DOI: [10.1103/PhysRevB.108.L060101](https://doi.org/10.1103/PhysRevB.108.L060101)

The effective Hamilton (H_{eff}) based on first-principles calculations has been successfully used to simulate ferroelectric phase transitions by statistical approaches, such as the Monte Carlo (MC) method, without any empirical or semiempirical coefficients [1–18]. The crucial advantage of H_{eff} is that it can be formulated flexibly by the expansion in power of the order parameters to describe the short-range interaction between the nearest neighbors, long-range interactions, and the couplings between different order parameters. This has reproduced and predicted the phase transitions of ferroelectrics in which the couplings are complex, especially for those with subtle intermediate phases involving small energy differences [19–21].

A discrepancy still exists, however, between the theoretical and experimental phase transition temperatures. The most common drawback of the H_{eff} -based MC simulations is the underestimated or overestimated phase transition temperature, which is generally attributed to the deviation of the lattice constant from the experimental value. Apart from improving the accuracy of exchange-correlation functionals [10], two adjustments have been made most often: (1) negative hydrostatic pressure [5,9] and (2) coupling between the soft-mode phonon and high-frequency optical phonons [9,10,22]. Noted that those improvements have not solved the problem of accurately predicting phase transition temperatures, and information about the true fluctuations of the order parameter is also missing.

In the present study, we find that such discrepancy between the theoretical and experimental observations is due to the slight difference in the mathematical space between

the macroscopic phenomenological model and the microscopic statistical model at the singularity point of the phase transition. From the mathematical point of view, the mathematical space of the macroscopic phenomenological model derived from experimental observation is the $\{E_{\text{tot}}, u\}$ space with respect to the total energy E_{tot} and order parameter u , while the space of the microscopic statistical model is constructed by the MC algorithm based on the $\{\Delta E_{\text{tot}}, \Delta u\}$ space. The integral of the microscopic H_{eff} statistical model is generally believed to recover the thermodynamic potential of the macroscopic phenomenological model [23]. In fact, the two mathematical spaces are not identical. Thus, we compensate a statistical singularity energy for this slight difference of the mathematical space through a dynamic mechanical differential equation. We also show that this slight difference works only at the phase transition point.

In the framework of Landau-Devonshire's theory, the thermodynamic potential F at each temperature point T during the ferroelectric phase transition (including first-order and second-order transitions) is described as follows [24,25]:

$$F = \begin{cases} F_0 + A(T - T_0)u^2 + Bu^4 + Cu^6, & \text{first-order} \\ F_0 + A(T - T_C)u^2 + Bu^4, & \text{second-order} \end{cases}, \quad (1)$$

where F is the thermodynamic potential of the system, u is the amplitude of the local soft mode, T_0 is the Curie-Weiss temperature, and T_C is the Curie temperature ($T_0 = T_C$ in the case of second-order phase transition). The coefficients A , B , and C depend on experiments. By decreasing the temperature from a high-symmetry paraelectric phase to a low-symmetry ferroelectric phase, the total energy surface of F at $u = 0$ changes from minimum to maximum and crosses the singularity (see Fig. 1). From the viewpoint of modern algebraic geometry,

*These authors contributed equally to this work.

†Corresponding author: hua_ke@hit.edu.cn

‡Corresponding author: zhouyu@hit.edu.cn

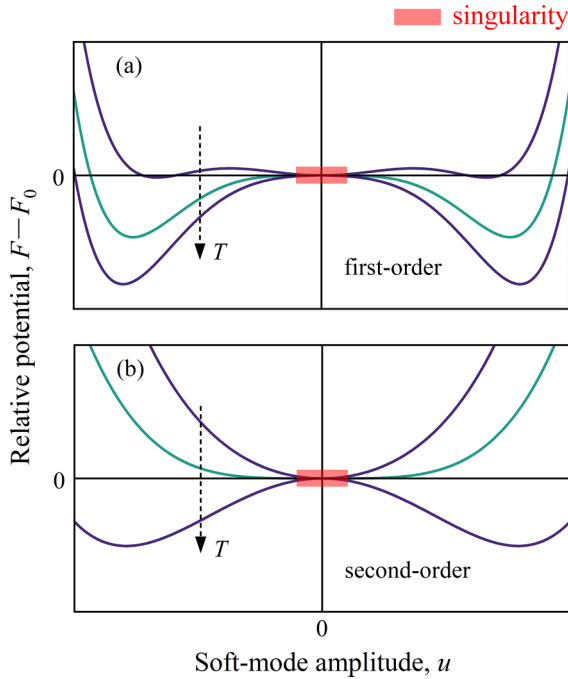


FIG. 1. Change of thermodynamic potential landscape from the high-symmetry paraelectric phase to the low-symmetry ferroelectric phase through (a) first-order phase transition and (b) second-order phase transition. The cyan lines are the potentials at (a) $T = T_0$ and (b) $T = T_C$. The singularity is marked as red segments.

the singularity derives from the “general point” that corresponds to the whole potential surface. For any infinitesimal temperature change $\Delta T = (T_1 - T_2) \rightarrow 0$, the property of the singularity depends on the intersection of the two potential surfaces of T_1 and T_2 . When T_1 and T_2 are away from the phase transition point (in the high-symmetry or low-symmetry phases), the intersection forms a point in which the $\{E_{\text{tot}}, u\}$ space constructed by the statistical $\{\Delta E_{\text{tot}}, \Delta u\}$ space fully reproduces the $\{E_{\text{tot}}, u\}$ space of the macroscopic thermodynamic potential. As ΔT crosses the phase transition point, the intersection expands to an infinitesimal segment, resulting in the slight difference between the constructed $\{E_{\text{tot}}, u\}$ space and the macroscopic $\{E_{\text{tot}}, u\}$ space.

Near the phase transition point, a finite Δu causes an error of the total energy, which could be regarded as the perturbation of an external field to the system [23]:

$$\Delta F = \frac{1}{2}(u - \bar{u})^2 \frac{\partial^2 F}{\partial u^2} = \frac{1}{2}(\Delta u)^2 \frac{\partial^2 F}{\partial u^2}, \quad (2)$$

where \bar{u} is the equilibrium value of u , and ΔF represents the minimum work needed to bring the system out of equilibrium [23]. In the original MC algorithm, the transition probability of a move Δu in i th unit cell is

$$p_i = \frac{\exp[-\beta E_{\text{tot},i}(u_i + \Delta u_i)]/Z}{\exp[-\beta E_{\text{tot},i}(u_i)]/Z} = \exp\{-\beta[E_{\text{tot},i}(u_i + \Delta u_i) - E_{\text{tot},i}(u_i)]\}, \quad (3)$$

where $Z = \sum_{i=1}^N \exp[-\beta E_{\text{tot},i}(u_i)]$ is the partition function, N is the number of unit cells in the system, and

$\beta = (k_B T)^{-1}$ with the Boltzmann constant k_B . Thus, the actual transition probability near the phase transition point should be

$$p_i = \exp\{-\beta[E_{\text{tot},i}(u_i + \Delta u_i) - E_{\text{tot},i}(u_i) + \Delta F]\}. \quad (4)$$

In Eq. (2), the $1/2(\Delta u)^2$ is the statistical bias, and the second partial derivative is the coefficient of ΔF and is positive throughout the temperature range. The latter can be obtained through first-principles calculation s:

$$\begin{aligned} \Delta F &= \frac{1}{2}(\Delta u_i)^2 \frac{\partial^2 E_{\text{tot}}}{\partial u^2} \\ &= \frac{1}{2}(\Delta u_i)^2 [2\kappa + 12\alpha u^2 + 30k_1 u^4 + 56k_4 u^6]. \end{aligned} \quad (5)$$

The coefficients in Eq. (5) are derived from the second partial derivative of H_{eff} with respect to u , which will be explained next.

Exemplified by the ferroelectric perovskites BaTiO_3 and PbTiO_3 , the total energy of the H_{eff} includes the local soft modes $\{\mathbf{u}_i\}$ with $\mathbf{u}_i = (u_{ix}, u_{iy}, u_{iz})$ and the strain tensor $\{\eta\}$, which is given by Ref. [5]:

$$\begin{aligned} E_{\text{tot}}(\{\mathbf{u}_i\}, \{\eta\}) &= E(\{\mathbf{u}_i\}) + E(\{\eta\}) + E(\{\mathbf{u}_i\}, \{\eta\}) \\ &= E_{\text{self}}(\{\mathbf{u}_i\}) + E_{\text{short}}(\{\mathbf{u}_i\}) + E_{\text{dpl}}(\{\mathbf{u}_i\}) \\ &\quad + E_{\text{elastic}}(\{\eta\}) + E_{\text{int}}(\{\mathbf{u}_i\}, \{\eta\}), \end{aligned} \quad (6)$$

where $E_{\text{self}}(\{\mathbf{u}_i\})$ is the in-site energy of local soft modes; $E_{\text{short}}(\{\mathbf{u}_i\})$ and $E_{\text{dpl}}(\{\mathbf{u}_i\})$ are the short-range interaction between nearest neighbors and the long-range dipole interaction of local soft modes, respectively; $E_{\text{elastic}}(\{\eta\})$ is the energy of homogeneous strain tensor; and $E_{\text{int}}(\{\mathbf{u}_i\}, \{\eta\})$ is the energy of the coupling between the local soft modes and homogeneous strain tensor. The κ in Eq. (5) is the quadratic coefficient of $E(\{\mathbf{u}_i\})$ in Eq. (6), including the quadratic terms of $E_{\text{self}}(\{\mathbf{u}_i\})$, $E_{\text{short}}(\{\mathbf{u}_i\})$, and $E_{\text{dpl}}(\{\mathbf{u}_i\})$. The coefficients of the quartic term and higher order terms are from the $E_{\text{self}}(\{\mathbf{u}_i\})$ as given by Ref. [9]:

$$\begin{aligned} E_{\text{self}}(\{\mathbf{u}_i\}) &= \sum_i E_{\text{self}}(\mathbf{u}_i) \\ &= \sum_i \{ \kappa_2 u_i^2 + \alpha u_i^4 + \gamma (u_{ix}^2 u_{iy}^2 + u_{iy}^2 u_{iz}^2 + u_{iz}^2 u_{ix}^2) \\ &\quad + k_1 u_i^6 + k_2 [u_{ix}^4 (u_{iy}^2 + u_{iz}^2) + u_{iy}^4 (u_{iz}^2 + u_{ix}^2) \\ &\quad + u_{iz}^4 (u_{ix}^2 + u_{iy}^2)] + k_3 u_{ix}^2 u_{iy}^2 u_{iz}^2 + k_4 u_i^8 \}. \end{aligned} \quad (7)$$

We determine the parametrization of H_{eff} by performing density-functional theory (DFT) calculations [26,27] within generalized gradient approximation (GGA) [28] with the Perdew-Burke-Ernzerhof parametrization revised for solids (PBEsol) [29], using Quantum ESPRESSO code [30,31]. In particular, we use the climbing image-nudged elastic band (CI-NEB) [32,33] method in the first-principles calculations to determine the coefficients k_1 , k_2 , k_3 , and k_4 of the coupling between soft-mode phonon and high-frequency optical phonons. For the MC simulations, we use the supercell system of $N = L_x \times L_y \times L_z = 14 \times 14 \times 14$ to compute the finite-temperature properties under heating and cooling processes.

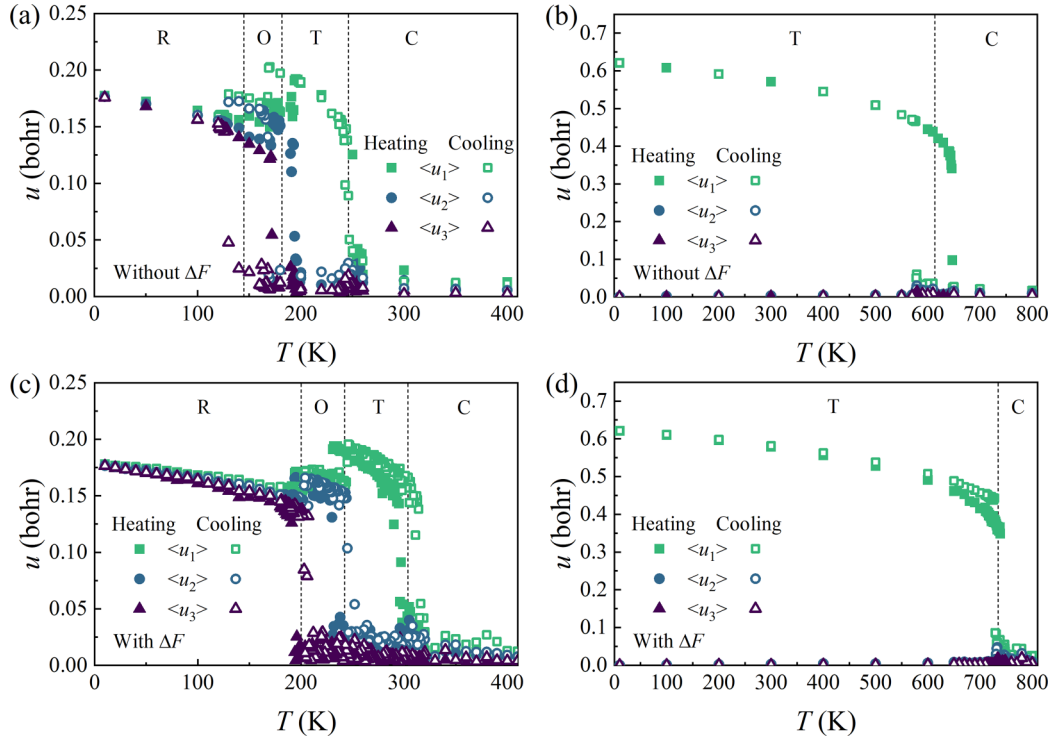


FIG. 2. Dependence of the supercell average $\langle \mathbf{u} \rangle$ on the temperature of BaTiO₃ and PbTiO₃ in [(a),(b)] the original MC method and [(c),(d)] the MC method with singularity energy compensation. The value of the maximum, middle, and minimum components of the supercell average $\langle \mathbf{u} \rangle$ is denoted as $\langle u_1 \rangle$, $\langle u_2 \rangle$, and $\langle u_3 \rangle$, respectively. The phases are distinguished by the dashed lines. Heating (solid) and cooling (hollow) sequences are shown.

Near the phase transition points, we use the temperature step of ± 1 K and 30 000 MC sweeps per temperature step in both heating and cooling sequences. Additional computational details are presented in the Supplemental Material [34].

To include singularity energy specifically in the transition probability as proposed in Eq. (4), the value of second partial derivative for the heating and cooling sequences in Eq. (5) is determined by the u when the transition is complete, as follows:

$$\frac{\partial^2 E_{\text{tot}}}{\partial u^2} = \begin{cases} \left. \frac{\partial^2 E_{\text{tot}}}{\partial u^2} \right|_{u=0} = |2\kappa|, & \text{heating} \\ \left. \frac{\partial^2 E_{\text{tot}}}{\partial u^2} \right|_{u=u_{\text{max}}} = |2\kappa + 12\alpha u_{\text{max}}^2 + 30k_1 u_{\text{max}}^4 + 56k_4 u_{\text{max}}^6|, & \text{cooling} \end{cases}, \quad (8)$$

where $u = 0$ and $u = u_{\text{max}}$ are determined by $\partial E_{\text{tot}}/\partial u = 0$ at the maximum and the minimum of the total energy E_{tot} based on first-principles calculations, respectively. We fix the value of second partial derivative over the whole temperature range and limit the singularity energy compensation corresponding to the maximum value of the move Δu to no more than $\hbar\omega$ (i.e., the energy of the soft-mode eigenfrequency). Therefore, the compensation only affects the transition probability and corrects the transition temperature near the phase transition point, where the fluctuation of u is equivalent to the magnitude of Δu . Far from the transition point, where u is zero or a finite value, the influence of the singularity energy compensation on the transition probability does not change the statistical distribution of u at that temperature. Because each trial move of \mathbf{u}_i in the MC algorithm is only in one direction, the singularity energy compensation is applied to the corresponding \mathbf{u}_i component (Δu_{ix} , Δu_{iy} , or Δu_{iz}) in each move.

We employ this simulation approach to compute the zero-pressure ferroelectric phase transition temperatures of BaTiO₃ and PbTiO₃, as shown in Table I. For clarity, the phase transition temperatures yielded by MC simulation are all considered to be Curie temperature T_C . Figure 2 shows the supercell average $\langle \mathbf{u} \rangle$ of the $\{\mathbf{u}_i\}$ as a function of temperature for BaTiO₃ and PbTiO₃. With decreasing temperature, BaTiO₃ experiences three transitions in the order of cubic (C), tetragonal (T), orthorhombic (O), and rhombohedral (R) phases, and PbTiO₃ experiences one transition from cubic to tetragonal phases. Comparing the transition temperatures with and without ΔF , the simulated temperatures are very close to the experimental values for the two materials after the singularity energy compensation. Specifically, the T_C of PbTiO₃ is in good agreement with experimental observation compared with previous results. This justifies the applicable compensation of singularity energy to improve the accuracy of

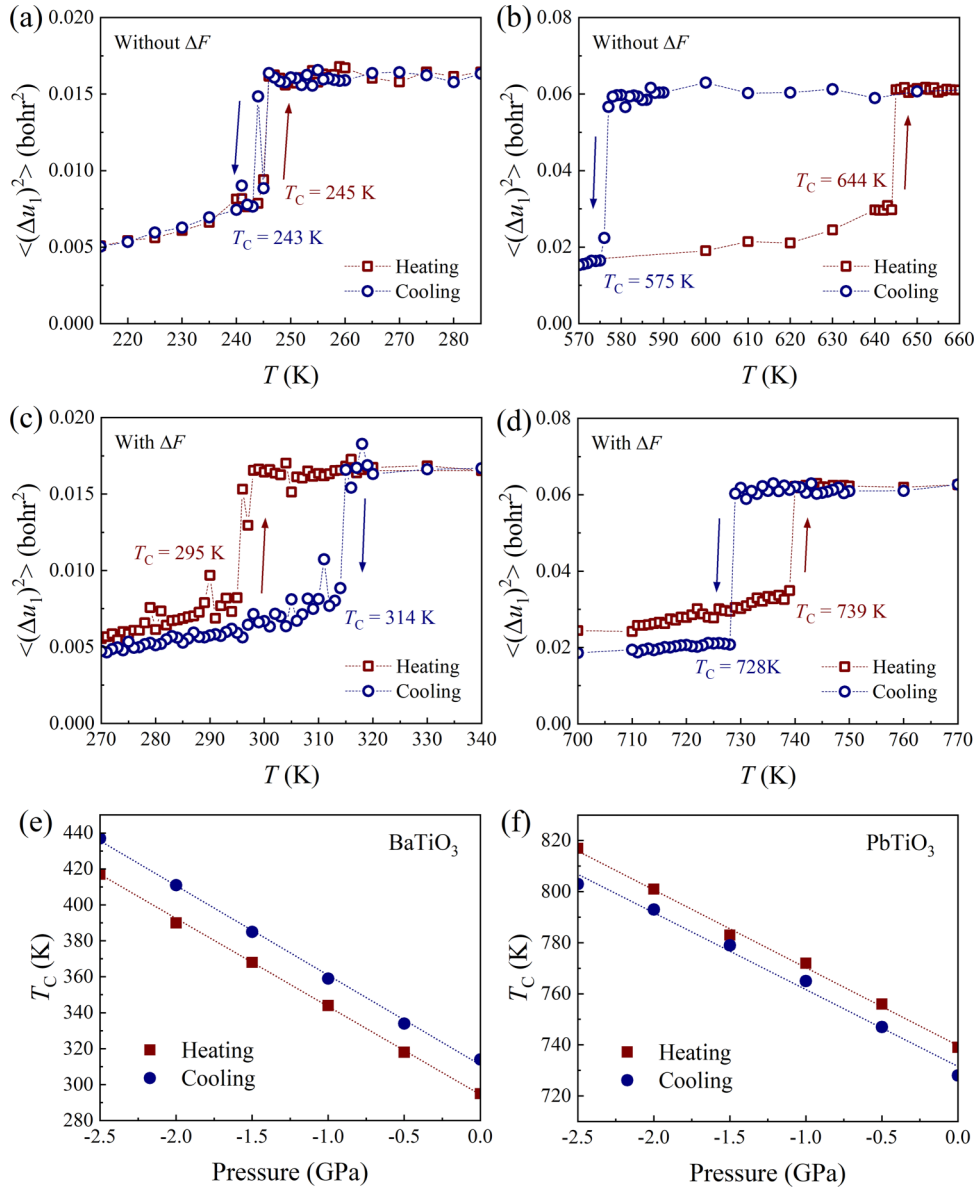


FIG. 3. Mean square fluctuations of BaTiO₃ and PbTiO₃ in the $T \leftrightarrow C$ phase transition obtained by [(a),(b)] the original MC method and [(c),(d)] the MC method with singularity energy compensation. The T_C of $T \leftrightarrow C$ phase transition for (e) BaTiO₃ and (f) PbTiO₃ varying with negative hydrostatic pressure after singularity energy compensation is shown.

TABLE I. Calculated phase transition temperatures (K) of BaTiO₃ and PbTiO₃ under zero external pressure. The data of this work are obtained under heating (cooling) sequence.

Compound	$R \leftrightarrow O$	$O \leftrightarrow T$	$T \leftrightarrow C$	Interpretation
BaTiO ₃	193 (202)	230 (244)	295 (314)	this work (with ΔF)
	173 (130)	195 (169)	245 (243)	this work (without ΔF)
	230	278	375	[10]
	102	160	288	[9]
	200	230	297	[4] (-4.8 GPa)
	183	278	403	expt. [35]
PbTiO ₃			739 (728)	this work (with ΔF)
			644 (575)	this work (without ΔF)
			675	[10]
			625	[11]
			635	[36,37] (experimental lattice constant)
		763	expt. [38]	

simulated phase transition temperatures for the MC method. When it is close to T_C , the singularity energy compensation increases the transition temperature towards the experimental value by adjusting the transition probability as in Eq. (4). Compared with the previous corrections of negative pressure [5,9] and high-frequency phonon coupling [9,10,22], the singularity energy compensation is fundamentally different. The negative pressure enhances the coupling between the soft mode and the strain, and the introduction of high-frequency phonons corrects the higher order anharmonic term of the soft mode. Those corrections improve the accuracy of simulated phase transition temperatures by increasing the energy difference of the H_{eff} in the transfer probability, without considering the anomaly of the transition probability at the singularity when approaching T_C in the statistical space.

We then explore the influence of singularity energy on the fluctuation near the $T \leftrightarrow C$ phase transition point of BaTiO₃ and PbTiO₃. We first study the mean square fluctuation of the $\langle u_1 \rangle$ component around T_C , where the $T \leftrightarrow C$ phase transition takes place as shown in Fig. 3. The fluctuation in the paraelectric cubic phase is larger than that in the ferroelectric tetragonal phase. The fluctuation in the ferroelectric phase is reduced to approximately half of that in the paraelectric phase within a small range near T_C , which corresponds to the relationship described by Landau [23]. For BaTiO₃, the thermal hysteresis after the singularity energy compensation is 19 K [Fig. 3(c)], which is better than 2 K before compensation [Fig. 3(a)], and the T_C of the cooling sequence is higher than that of the heating sequence. This phenomenon is consistent with the experimental observations that the cooling T_C is higher than the heating T_C and the thermal hysteresis of ~ 6 K [39]. For PbTiO₃, the thermal hysteresis after singularity energy compensation is 11 K [Fig. 3(d)], which is less than 69 K before compensation [Fig. 3(b)] but more consistent with the experimental value of ~ 7 K [40].

The effect of negative hydrostatic pressure on the T_C of $T \leftrightarrow C$ phase transition is shown in Figs. 3(e) and 3(f). For both BaTiO₃ and PbTiO₃, the simulated T_C has a linear relationship with pressure. The slopes dT_C/dP in the heating and cooling sequence are nearly the same. The average dT_C/dP for BaTiO₃ and PbTiO₃ is 49.4 and 30.3 K/GPa, respectively, which is in agreement with experimental values of 52 and 84 K/GPa, respectively [41]. The discrepancy for PbTiO₃ may be due to the fact that the experimental data are obtained under positive pressure [41].

Finally, we study the influence of singularity energy on the mean square fluctuation of soft-mode $\mathbf{u}(\mathbf{k})$ in reciprocal space near the $T \leftrightarrow C$ phase transition, which we use to evaluate the order-disorder degree of the soft mode near the phase transition point. Following the treatment in Ref. [5], the average Fourier modulus $F(\mathbf{k}, T) = \langle |\mathbf{u}(\mathbf{k})|^2 \rangle$ represents the mean square fluctuation. We calculate the mode hardness quantity $\rho(\mathbf{k}) = 2\omega^2(\mathbf{k}, T)/\omega^2(\mathbf{k}, 2T)$ of the LO, TO1, and TO2 branches of the soft mode, where T is any temperature higher than T_C and the square of the eigenfrequency $\omega^2(\mathbf{k})$ is proportional to $T/F(\mathbf{k}, T)$ [5]. Figure 4 shows the $\rho(\mathbf{k})$ of the optical transverse TO1 and TO2 modes along the pathway of high-symmetry Γ , X, M, and R points in the Brillouin zone (BZ) for cubic BaTiO₃ and PbTiO₃, with T being 400 and 850 K, respectively. The optical longitudinal

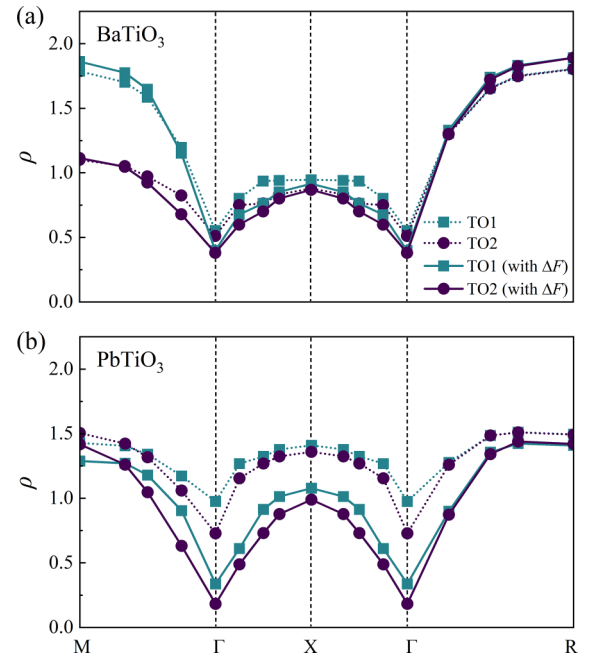


FIG. 4. Mode hardness quantity $\rho(\mathbf{k})$ of TO1 and TO2 modes for (a) BaTiO₃ and (b) PbTiO₃ along the high-symmetry directions in the BZ. The $\rho(\mathbf{k})$ of the heating sequence is shown, whose trend is the same as that of the cooling sequence.

LO mode is omitted. An optical branch is considered soft if its $\rho(\mathbf{k}) < 1$, and the extent to which it expands in the BZ determines the degree of order-disorder [5]. As shown in Fig. 4(a), the TO1 and TO2 modes quickly harden at the zone boundary M and R points while they remain soft along the Γ -X direction, indicating a partial order-disorder character of $T \leftrightarrow C$ transition for BaTiO₃. After compensating the singularity energy, the $\rho(\mathbf{k})$ of both TO1 and TO2 modes along the Γ -X direction is reduced, which confirms that the degree of order-disorder character is enhanced. In Fig. 4(b), TO1 and TO2 modes quickly harden throughout the BZ, indicating a full displacive character in the $T \leftrightarrow C$ transition for PbTiO₃. After the compensation of singularity energy, the order-disorder character emerges as the $\rho(\mathbf{k})$ of TO1 and TO2 modes along the Γ -X direction is reduced below 1. This result conforms to the experimental observation that the $T \leftrightarrow C$ transition of PbTiO₃ demonstrates a strong degree of order-disorder [42–45].

In summary, we compensate for the slight difference in mathematical space between the macroscopic phenomenological model and the microscopic statistical model at the singularity of phase transition point by means of statistical singularity energy in H_{eff} -based MC simulations of ferroelectric phase transition. The phase transition temperatures of BaTiO₃ and PbTiO₃ have good consistency with the experimental results. Near the $T \leftrightarrow C$ phase transition point, we accurately evaluate the thermal hysteresis and the order-disorder degree of the soft mode by the fluctuation of the soft mode in the real space and the reciprocal space. Our method is expected to be applied to complex phase transitions with multiple singularities (sometimes the singularities are of different spaces).

We would like to thank D. Vanderbilt for providing invaluable guidance on the details of H_{eff} and Monte Carlo simulation method. We also acknowledge the tremendous inspiration

by the authors and contributors in the references. This work was supported by National Natural Science Foundation of China (Grants No. 51772065 and No. 52111530040).

-
- [1] K. M. Rabe and J. D. Joannopoulos, *Ab Initio* Determination of a Structural Phase Transition Temperature, *Phys. Rev. Lett.* **59**, 570 (1987).
- [2] K. M. Rabe and U. V. Waghmare, First-principles model hamiltonians for ferroelectric phase transitions, *Ferroelectrics* **136**, 147 (1992).
- [3] R. D. King-Smith and D. Vanderbilt, First-principles investigation of ferroelectricity in perovskite compounds, *Phys. Rev. B* **49**, 5828 (1994).
- [4] W. Zhong, D. Vanderbilt, and K. M. Rabe, Phase Transitions in BaTiO_3 from First Principles, *Phys. Rev. Lett.* **73**, 1861 (1994).
- [5] W. Zhong, D. Vanderbilt, and K. M. Rabe, First-principles theory of ferroelectric phase transitions for perovskites: The case of BaTiO_3 , *Phys. Rev. B* **52**, 6301 (1995).
- [6] I. A. Kornev, L. Bellaiche, P. E. Janolin, B. Dkhil, and E. Suard, Phase Diagram of $\text{Pb}(\text{Zr}, \text{Ti})\text{O}_3$ Solid Solutions from First Principles, *Phys. Rev. Lett.* **97**, 157601 (2006).
- [7] I. A. Kornev, S. Lisenkov, R. Haumont, B. Dkhil, and L. Bellaiche, Finite-Temperature Properties of Multiferroic BiFeO_3 , *Phys. Rev. Lett.* **99**, 227602 (2007).
- [8] T. Nishimatsu, U. V. Waghmare, Y. Kawazoe, and D. Vanderbilt, Fast molecular-dynamics simulation for ferroelectric thin-film capacitors using a first-principles effective Hamiltonian, *Phys. Rev. B* **78**, 104104 (2008).
- [9] T. Nishimatsu, M. Iwamoto, Y. Kawazoe, and U. V. Waghmare, First-principles accurate total energy surfaces for polar structural distortions of BaTiO_3 , PbTiO_3 , and SrTiO_3 : Consequences for structural transition temperatures, *Phys. Rev. B* **82**, 134106 (2010).
- [10] A. Paul, J. Sun, J. P. Perdew, and U. V. Waghmare, Accuracy of first-principles interatomic interactions and predictions of ferroelectric phase transitions in perovskite oxides: Energy functional and effective Hamiltonian, *Phys. Rev. B* **95**, 054111 (2017).
- [11] B. K. Mani, C. M. Chang, and I. Ponomareva, Atomistic study of soft-mode dynamics in PbTiO_3 , *Phys. Rev. B* **88**, 064306 (2013).
- [12] L. Bellaiche, A. García, and D. Vanderbilt, Finite-Temperature Properties of $\text{Pb}(\text{Zr}_{1-x}\text{Ti}_x)\text{O}_3$ Alloys from First Principles, *Phys. Rev. Lett.* **84**, 5427 (2000).
- [13] D. Vanderbilt and W. Zhong, First-principles theory of structural phase transitions for perovskites: Competing instabilities, *Ferroelectrics* **206**, 181 (1998).
- [14] H. J. Xiang, S. H. Wei, and M. H. Whangbo, Origin of the Structural and Magnetic Anomalies of the Layered Compound SrFeO_2 : A Density Functional Investigation, *Phys. Rev. Lett.* **100**, 167207 (2008).
- [15] B. K. Mani, S. Lisenkov, and I. Ponomareva, Finite-temperature properties of antiferroelectric PbZrO_3 from atomistic simulations, *Phys. Rev. B* **91**, 134112 (2015).
- [16] C.-M. Chang, B. Mani, S. Lisenkov, and I. Ponomareva, Prediction of electromagnons in antiferromagnetic ferroelectrics from first-principles: The case of BiFeO_3 , *Ferroelectrics* **494**, 68 (2016).
- [17] S. H. Skjærvø, Q. N. Meier, M. Feygenson, N. A. Spaldin, S. J. L. Billinge, E. S. Bozin, and S. M. Selbach, Unconventional Continuous Structural Disorder at the Order-Disorder Phase Transition in the Hexagonal Manganites, *Phys. Rev. X* **9**, 031001 (2019).
- [18] D. Albrecht, S. Lisenkov, W. Ren, D. Rahmedov, I. A. Kornev, and L. Bellaiche, Ferromagnetism in multiferroic BiFeO_3 films: A first-principles-based study, *Phys. Rev. B* **81**, 140401(R) (2010).
- [19] S. Prosandeev, D. Wang, W. Ren, J. Íñiguez, and L. Bellaiche, Novel nanoscale twinned phases in perovskite oxides, *Adv. Funct. Mater.* **23**, 234 (2013).
- [20] B. Xu, D. Wang, J. Íñiguez, and L. Bellaiche, Finite-temperature properties of rare-earth-substituted BiFeO_3 multiferroic solid solutions, *Adv. Funct. Mater.* **25**, 552 (2015).
- [21] Y. Yang, B. Xu, C. Xu, W. Ren, and L. Bellaiche, Understanding and revisiting the most complex perovskite system via atomistic simulations, *Phys. Rev. B* **97**, 174106 (2018).
- [22] T. Hashimoto, T. Nishimatsu, H. Mizuseki, Y. Kawazoe, A. Sasaki, and Y. Ikeda, *Ab initio* determination of total-energy surfaces for distortions of ferroelectric perovskite oxides, *Jpn. J. Appl. Phys.* **43**, 6785 (2004).
- [23] L. D. Landau and E. M. Lifshitz, *Statistical Physics* (Pergamon, Oxford, 1980).
- [24] L. D. Landau, On the theory of phase transitions I, *Zh. Eksp. Teor. Fiz.* **11**, 19 (1937).
- [25] A. F. Devonshire, XCVI. Theory of barium titanate, *Philos. Mag.* **40**, 1040 (1949).
- [26] P. Hohenberg and W. Kohn, Inhomogeneous electron gas, *Phys. Rev.* **136**, B864 (1964).
- [27] W. Kohn and L. J. Sham, Self-consistent equations including exchange and correlation effects, *Phys. Rev.* **140**, A1133 (1965).
- [28] J. P. Perdew, K. Burke, and M. Ernzerhof, Generalized Gradient Approximation Made Simple, *Phys. Rev. Lett.* **77**, 3865 (1996).
- [29] J. P. Perdew, A. Ruzsinszky, G. I. Csonka, O. A. Vydrov, G. E. Scuseria, L. A. Constantin, X. Zhou, and K. Burke, Restoring the Density-Gradient Expansion for Exchange in Solids and Surfaces, *Phys. Rev. Lett.* **100**, 136406 (2008).
- [30] P. Giannozzi, S. Baroni, N. Bonini, M. Calandra, R. Car, C. Cavazzoni, D. Ceresoli, G. L. Chiarotti, M. Cococcioni, I. Dabo *et al.*, QUANTUM ESPRESSO: A modular and open-source software project for quantum simulations of materials, *J. Phys.: Condens. Matter* **21**, 395502 (2009).
- [31] P. Giannozzi, O. Andreussi, T. Brumme, O. Bunau, M. B. Nardelli, M. Calandra, R. Car, C. Cavazzoni, D. Ceresoli, M. Cococcioni *et al.*, Advanced capabilities for materials modelling with Quantum ESPRESSO, *J. Phys.: Condens. Matter* **29**, 465901 (2017).
- [32] G. Henkelman, B. P. Uberuaga, and H. Jónsson, A climbing image nudged elastic band method for finding saddle points and minimum energy paths, *J. Chem. Phys.* **113**, 9901 (2000).
- [33] D. Sheppard, R. Terrell, and G. Henkelman, Optimization methods for finding minimum energy paths, *J. Chem. Phys.* **128**, 134106 (2008).

- [34] See Supplemental Material at <http://link.aps.org/supplemental/10.1103/PhysRevB.108.L060101> for more details about the first-principles calculations and the CI-NEB method. Extra Monte Carlo (MC) simulation results of mean square fluctuation of BaTiO₃ and PbTiO₃, negative-pressure-dependent T_C of BaTiO₃, and mode hardness quantity $\rho(\mathbf{k})$ of the cooling sequence are also given.
- [35] C. J. Johnson, Some dielectric and electro-optic properties of BaTiO₃ single crystals, *Appl. Phys. Lett.* **7**, 221 (1965).
- [36] U. V. Waghmare and K. M. Rabe, *Ab initio* statistical mechanics of the ferroelectric phase transition in PbTiO₃, *Phys. Rev. B* **55**, 6161 (1997).
- [37] T. Nishimatsu, K. Aoyagi, T. Kiguchi, T. J. Konno, Y. Kawazoe, H. Funakubo, A. Kumar, and U. V. Waghmare, Molecular dynamics simulation of 90° ferroelectric domains in PbTiO₃, *J. Phys. Soc. Jpn.* **81**, 124702 (2012).
- [38] G. Shirane, R. Pepinsky, and B. C. Frazer, X-ray and neutron diffraction study of ferroelectric PbTiO₃, *Acta Crystallogr.* **9**, 131 (1956).
- [39] J. Suchanicz, G. Stopa, K. Konieczny, D. Wcisło, M. Dziubaniuk, and J. Rymarczyk, Uniaxial pressure effect on the dielectric properties of the BaTiO₃ single crystals, *Ferroelectrics* **366**, 3 (2008).
- [40] B. N. Sun, Y. Huang, and D. A. Payne, Growth of large PbTiO₃ crystals by a self-flux technique, *J. Cryst. Growth* **128**, 867 (1993).
- [41] G. A. Samara, Pressure and temperature dependence of the dielectric properties and phase transitions of the ferroelectric perovskites: PbTiO₃ and BaTiO₃, *Ferroelectrics* **2**, 277 (1971).
- [42] M. D. Fontana, H. Idrissi, and K. Wojcik, Displacive to order-disorder crossover in the cubic-tetragonal phase transition of PbTiO₃, *Europhys. Lett.* **11**, 419 (1990).
- [43] R. J. Nelmes, R. O. Piltz, W. F. Kuhs, Z. Tun, and R. Restori, Order-disorder behaviour in the transition of PbTiO₃, *Ferroelectrics* **108**, 165 (1990).
- [44] B. Ravel, N. Scleron, Y. Yacoby, E. A. Stern, F. Dogan, and J. J. Rehr, Order-disorder behavior in the phase transition of PbTiO₃, *Ferroelectrics* **164**, 265 (1995).
- [45] Y.-H. Shin, J.-Y. Son, B.-J. Lee, I. Grinberg, and A. M. Rappe, Order-disorder character of PbTiO₃, *J. Phys.: Condens. Matter* **20**, 015224 (2008).